


Waveguide-Invariant-Based Ranging and Receiver Localization Using Tonal Sources of Opportunity

Andrew H. Young, H. Andrew Harms, Granger W. Hickman, Jeffrey S. Rogers , *Member, IEEE*,
and Jeffrey L. Krolik, *Senior Member, IEEE*

Abstract—Acoustic emissions from cargo ships transiting coastal waterways, measured by a single hydrophone, can be exploited to estimate both the time-varying source–receiver range and receiver location. In this paper, two parameter-search-based maximum-likelihood estimators are presented: one for β , the waveguide invariant parameter, and one for source range. β characterizes the interference structure inherent to ducted acoustic propagation and is central to the spectral analysis involved in the range estimation. The source ranging method extends prior work by the authors and focuses on the strong narrowband tonals that typically dominate the acoustic spectra of cargo ships. Source ranging results are presented using real data from the SWellEx-96 experiment and are shown to be in close agreement with simulation results obtained using the KRAKEN normal mode program. A technique for estimating the position of a receiver, which can be stationary or moving, is also proposed. The localization technique requires knowledge of the source track, hydrophone data, and an initial estimate of the receiver’s position. An application to autonomous underwater vehicle (AUV) navigation is included in which the waveguide-invariant-based range estimates are used to mitigate the position estimation error due to drift in inertial measurement units on submerged AUVs. A specific scenario is examined, using SWellEx-96 data, in which an initial position error of 3 km is reduced to under 1 km using the proposed technique.

Index Terms—Receiver localization, source ranging, shallow water, tonal source, waveguide invariant.

I. INTRODUCTION

AUTONOMOUS underwater vehicle (AUV) localization is a difficult problem, primarily due to the inability of Global Positioning System (GPS) signals to propagate significant distances in ocean water. Without GPS, AUVs rely on a variety of systems spanning a range of cost and complexity, including inertial measurement units (IMUs), Doppler velocity loggers

Manuscript received May 17, 2018; revised September 13, 2018; accepted November 19, 2018. Date of publication January 31, 2019; date of current version April 14, 2020. This work was supported by the Office of Naval Research. (Corresponding author: Andrew H. Young.)

Associate Editor: B. Nicolas.

A. H. Young is with the Department of Electrical and Computer Engineering, Duke University, Durham, NC 27708 USA, and also with the Acoustics Division, Code 7164, Naval Research Laboratory, Washington, DC 20375 USA (e-mail: ayounge.ece@duke.edu).

H. A. Harms is with the Department of Electrical and Computer Engineering, University of Nebraska-Lincoln, Lincoln, NE 68588 USA (e-mail: harms@unl.edu).

G. W. Hickman and J. L. Krolik are with the Department of Electrical and Computer Engineering, Duke University, Durham, NC 27708 USA (e-mail: granger.hickman@duke.edu; jlk@duke.edu).

J. S. Rogers is with the Acoustics Division, Code 7164, Naval Research Laboratory, Washington, DC 20375 USA (e-mail: jeff.rogers@nrl.navy.mil).

Digital Object Identifier 10.1109/JOE.2018.2883855

(DVLs), and transponders in either a long baseline or ultrashort baseline configuration [1], and each type of equipment comes with a unique set of advantages and limitations. One of the aims of this paper is to validate single hydrophone, waveguide-invariant-based acoustic source ranging techniques as a viable addition to this list. To this end, a passive localization technique is presented that requires minimal, low-cost equipment and can potentially enable AUVs to remain submerged indefinitely in coastal shipping lanes while maintaining a bounded position error.

The waveguide invariant, commonly denoted by β , is a scalar parameter that characterizes the striations, or lines of constant intensity, exhibited in spectrograms of acoustic data acquired in ocean environments. The parameter was first described by Chuprov [2], who presented it in the context of the readily observable interference structures that result from the coherent addition of propagating modes in a ducted environment. For a broadband source in shallow water, the interference structures can be observed in a plot of the acoustic intensity at a single hydrophone as a function of source–receiver range r and radial frequency ω . Such a plot is herein referred to as an $I(r, \omega)$ surface, and a clear example is provided in Fig. 1(a) for a broadband source in a shallow-water environment characterized by $\beta = 1$. When the time-varying range to a transiting broadband source is known, the $I(r, \omega)$ surface is easily obtained by first computing the squared magnitude of a spectrogram of hydrophone data and subsequently mapping time to source range. For sources of opportunity (SOOs), such as cargo ships, this mapping can be performed using the automatic identification system (AIS) data they are required to broadcast while transiting coastal waterways [3].

Multiple techniques have been developed to leverage the striations observed in time–frequency spectrograms for the purpose of estimating source–receiver range, beginning in 2000 with Thode [4], who used a Radon transform technique applied to data from a vertical hydrophone array. However, when using only a single hydrophone to estimate source range, an estimate of the range rate is also required, and in 2007, Tao *et al.* [5] proposed a Hough-transform-based method for estimating the ratio of source velocity to range in cases where the source track exhibits the closest point of approach (CPA). Alternatively, the 2-D discrete Fourier transform (DFT) can be employed to estimate the slope $\Delta\omega/\Delta r$ of striations locally across the spectrogram when source range rate is known, as in the work by Cockrell and Schmidt [6] that does not require the CPA to be exhibited in the source track. Striation-based range estimation techniques

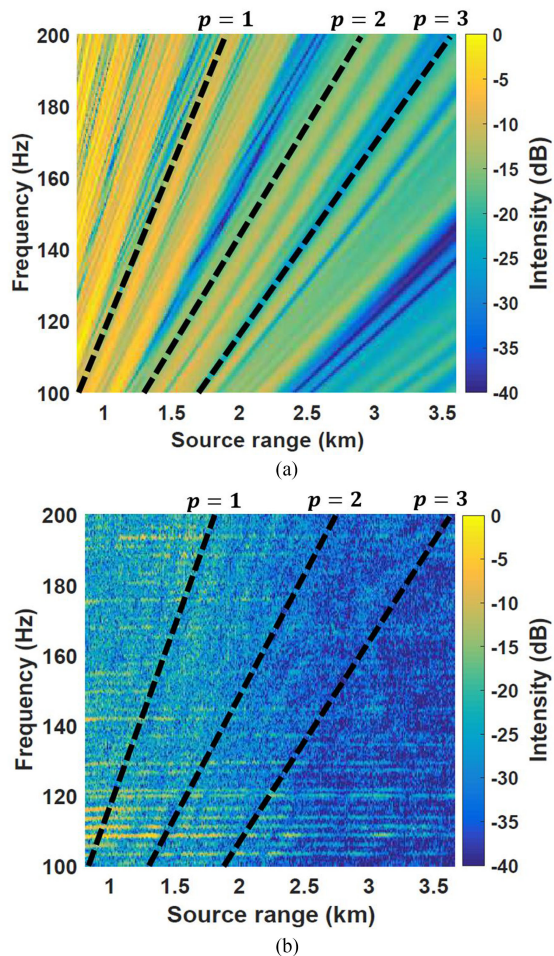


Fig. 1. Acoustic intensity at a single receiver plotted as a function of frequency and range to a transiting source. (a) Simulated broadband source in a Pekeris waveguide. (b) Real, tonal source (cargo ship) in a shallow-water environment from the Noise-09 experiment. In both cases, the striations, or lines of constant intensity, in the plots are generally characterized by $\beta = 1$, as seen by the agreement between the slopes of the striations and those of the three dashed lines obeying (7) and identified by $p = 1, 2, 3$ labels overlaid on each plot. The fading pattern is more difficult to see in (b) due to the mixture of strong tonal components with weaker, broadband components in the cargo ship acoustic emissions spectrum.

require estimates of the waveguide invariant parameter, and although the general $\beta = 1$ approximation is commonly employed in shallow-water environments, more accurate estimates of β for a particular environment can improve range estimation results, as noted by Turgut *et al.* [7] in their work that utilized striations observed in beam data from a horizontal line array to estimate source range.

When source range is known, β can be estimated by applying the same types of techniques used for range estimation, and notable early examples include the 2-D DFT-based techniques employed by Rouseff and Spindel [8] and Yang [9], as well as the normalized striation slope estimation technique of Heaney [10] and the minimum variance technique proposed by Brooks *et al.* [11]. Such image-processing-based techniques have been shown to work well for broadband sources in shallow-water environments, but their performance can be significantly degraded when applied to tonal sources.

Unfortunately, loud acoustic SOOs tend to have emissions spectra that are dominated by narrowband tonals [12], and the resulting $I(r, \omega)$ surface is not smoothly varying as it is for the broadband case shown in Fig. 1(a), but is instead more likely to resemble Fig. 1(b), which was obtained from hydrophone measurements of the acoustic emissions of a cargo ship transiting a shallow-water shipping lane off the coast of San Diego, California. The mixture of narrowband and broadband components significantly reduces the effectiveness of image processing techniques that inherently assume a uniform, broadband source spectrum. Motivated in part by the ubiquity of powerful, tonal acoustic radiators in the ocean, Verlinden *et al.* [13] have recently proposed a technique for mitigating the impact of the tonal components in SOO spectra to image-based processing techniques by removing them in the Radon transform domain and then estimating β from striations in the filtered $I(r, \omega)$ surface. This was shown to improve the ability to estimate striation slopes using the broadband spectral content, but it dismisses a wealth of environmental information encoded in the tonal components.

In this paper, a complementary β estimation technique is presented in which the tonal components are viewed as the signal, rather than as noise, and only striations in the strongest tones are considered by the processor. A general framework for estimating β from tones was introduced by Harms *et al.* [14], and this paper extends the signal model they developed to a maximum-likelihood (ML) framework for estimation of both β and source range. Range estimation using SOOs has a potentially significant application to AUV navigation, a concept which has been introduced in recent work by Young *et al.* [15]. In their paper, the authors investigated the feasibility of exploiting the waveguide invariant for AUV localization and proposed a simple, least-squares-based algorithm that utilizes waveguide-invariant-based source range estimates, AIS data, and the Doppler effect. In this paper, a similar technique, although one that does not utilize the Doppler effect, is presented. Results obtained using real data from the SWellEx-96 experiment highlight the potential for this technique to be used for localizing AUVs that have incurred substantial position uncertainty during the interval between deployment and recovery, either in real time or post-mission.

Derivations of the tonal-based techniques for ML estimation of β and source range are presented in Section II along with a validation of the β estimator using a simulated Pekeris waveguide. The performance of the estimators is evaluated using real data from the SWellEx-96 experiment, which is presented in Section III, and compared to simulation results obtained using KRAKEN. The application to AUV navigation, as well as receiver localization results obtained from processing SWellEx-96 data, is presented in Section IV, and key findings are summarized in Section V.

II. SIGNAL MODEL AND DERIVATION OF ESTIMATORS

This section begins with an introduction of the signal model that is used throughout this paper and then moves into specific derivations of the estimators for β , source range, and receiver position. The signal model described in Sections II-A and II-B borrows heavily from [14] but also extends the authors' prior work by adjusting for unequal tonal source levels and including an ML estimator for frequency-dependent noise variance.

A. Received Signal Model

The acoustic emissions spectra of cargo ships are generally dominated by narrowband tonals corresponding to fundamental and harmonic oscillations of rotary mechanical devices and structures such as onboard diesel generators, propulsion engines, and propellers [12]. Accordingly, the source signal $s(t)$ is modeled as a sum of K tones

$$s(t) = \sum_{k=1}^K A_k e^{j(\omega_k t + \phi_k)} \quad (1)$$

where k is the index of each tonal component, in ascending order according to radial frequency, and A_k is the amplitude of the k th tonal. The values A_k and ϕ_k correspond to pressure field magnitudes and phases, respectively, and are assumed constant, but unknown, over the observation interval. However, the phases ϕ_k do not have to be perfectly stable, as the processor only considers acoustic intensity, which is proportional to the square of the pressure magnitude, and discards the phase measurement of the received signal.

In the frequency domain, the signal received at a hydrophone due to a transiting, tonal SOO at range r can be expressed as follows:

$$Z(r, \omega) = \underbrace{S(\omega)H(r, \omega)}_{X(r, \omega)} + N(\omega) \quad (2)$$

where $S(\omega)$ represents the source spectrum, $H(r, \omega)$ is the channel response expressed as a function of frequency and source range, and $N(\omega)$ represents the frequency-dependent contribution from background noise sources. $X(r, \omega)$, which is the product of the channel response and the source spectrum, thus represents the source signal received at the hydrophone, whereas the noise $N(\omega)$ is modeled as a circularly symmetric Gaussian random variable consisting of independent real and imaginary components as follows:

$$\begin{aligned} N(\omega) &= N_R(\omega) + jN_I(\omega) \\ N_R(\omega), N_I(\omega) &\sim \mathcal{N}(0, \sigma_n^2(\omega)) \end{aligned} \quad (3)$$

where $\sigma_n^2(\omega)$ is a frequency-dependent noise variance. Let $Y(r, \omega)$ be defined as the ratio of the intensity of the received signal at a specific source range and frequency, $|Z(r, \omega)|^2$, to the noise variance, as follows:

$$\begin{aligned} Y(r, \omega) &\triangleq \frac{|Z(r, \omega)|^2}{\sigma_n^2(\omega)} \\ &= \left(\frac{X_R(r, \omega)}{\sigma_n(\omega)} + \frac{N_R(\omega)}{\sigma_n(\omega)} \right)^2 + \left(\frac{X_I(r, \omega)}{\sigma_n(\omega)} + \frac{N_I(\omega)}{\sigma_n(\omega)} \right)^2 \end{aligned} \quad (4)$$

where $X_R(r, \omega)$ and $X_I(r, \omega)$ denote the real and imaginary parts of $X(r, \omega)$, respectively. As a result of assuming constant, non-random source tone amplitudes A_k in (1), $Y(r, \omega)$ is noncentral chi-squared distributed with two degrees of freedom and will be represented by the random variable Y for ease of notation. The density function of Y is as follows [16]:

$$f_Y(y; \lambda) = \frac{1}{2} I_0 \left(\sqrt{\lambda y} \right) e^{-\frac{1}{2}(y+\lambda)} \quad (5)$$

where $I_0(\cdot)$ denotes a modified Bessel function of the first kind. The noncentrality parameter λ is given as follows:

$$\begin{aligned} \lambda &= \frac{X_R(r, \omega)^2}{\sigma_n^2(\omega)} + \frac{X_I(r, \omega)^2}{\sigma_n^2(\omega)} \\ &= \frac{I(r, \omega)}{\sigma_n^2(\omega)} \end{aligned} \quad (6)$$

where $I(r, \omega)$ is the intensity of the received acoustic signal due to the tonal source at range r and frequency ω and is represented as the squared magnitude of $X(r, \omega)$: $I(r, \omega) = |X(r, \omega)|^2$.

B. Modeling Intensity Along Striations

The statistical signal modeling presented in Section II-A allows for the fading observed in measured data to be attributed to channel effects rather than source generation, which is often the case in multipath environments. For multipath environments that are well characterized by a single value of β , the loci of points along striations in the fading pattern obey the following relationship [17]:

$$\frac{\omega}{\omega_0} = \left(\frac{r}{r_0} \right)^\beta. \quad (7)$$

Evaluation of the likelihood function from (5) for measurements along the loci given by (7) requires $\sigma_n^2(\omega)$ and $I(r, \omega)$, and methods for obtaining ML estimates of these parameters are now presented.

To estimate $\sigma_n^2(\omega)$, we begin by observing that under the assumption of complex Gaussian additive noise, the magnitude of $N(\omega)$ is Rayleigh distributed with scale parameter $\sigma_n(\omega)$ [18]. The parameter $\sigma_n^2(\omega)$ can be estimated directly from samples of the $Z(r, \omega)$ surface taken at frequencies that are adjacent to the source tonals, yet with sufficient separation as to have negligible contribution to the measured intensity, such that $|Z(r, \omega)| \approx |N(\omega)|$. In practice, there will also be a nonzero contribution from the broadband source emissions spectrum, and this is not explicitly accounted for under the model. Although such broadband noise has been noted to be approximately log-normal in distribution [19], rather than effectively having the Rayleigh distribution that is assumed under this signal model, the environmental noise arising from a multitude of point sources spread throughout the channel is herein assumed to generally dominate over the broadband vessel noise. Notable exceptions could include scenarios in which the source vessel is at close range, the signal contains very weak tonals, and when processing array data steered in the source direction. Therefore, broadband models might be profitably incorporated into this technique in future work to account for such cases.

The unbiased ML estimate [20] of $\sigma_n^2(\omega)$ is computed as follows:

$$\widehat{\sigma_n^2}(\omega) = \frac{1}{4M} \sum_{m=1}^M (|Z(r_m, \omega + \delta\omega)|^2 + |Z(r_m, \omega - \delta\omega)|^2) \quad (8)$$

where ω corresponds to one of the tonal frequencies, $\delta\omega$ is a small frequency offset, and M is the number of short-time Fourier transform frames in $Z(r, \omega)$. For an environment well

characterized by a scalar β , any striation projected through frequency and range in accordance with (7) using the correct value of β will have a constant value of $H(r, \omega)$ from (2). Therefore, the received intensities due to the signal $I(r, \omega)$ at each tonal frequency along a striation are related as follows:

$$\frac{I(r_k, \omega_k)}{I(r_l, \omega_l)} = \left(\frac{A_k}{A_l} \right)^2 \quad (9)$$

where A_k and A_l are the magnitudes of the k th and l th tones in the source signal described in (1), and r_k and r_l are the ranges along the striation corresponding to the k th and l th tones. Let α_k be defined as the ratio of the amplitude of the k th tone to the largest tonal amplitude, A_{\max} , as follows:

$$\alpha_k \triangleq \frac{A_k}{A_{\max}}. \quad (10)$$

The received signal intensities along a striation can then be written as follows:

$$I(r_k, \omega_k) = \alpha_k^2 I_{\max} \quad (11)$$

where I_{\max} is the maximum intensity along the striation. Along with the frequency-dependent noise variance estimates $\widehat{\sigma}_n^2(\omega)$, the signal intensities given by (11) allow the noncentrality parameter λ to be computed using (6), which enables (5) to be evaluated for the measured data. Given estimates of α_k and I_{\max} , the received signal intensities $I(r_k, \omega_k)$ along a striation can be estimated using (11), and methods for estimating those parameters are now covered, beginning with α_k .

Since the tonal amplitudes are assumed constant, the parameter α_k can be estimated for each tonal component by averaging the magnitudes of the corresponding spectral components over all M frames, as follows:

$$\hat{\alpha}_k = \frac{\sum_{m=1}^M |Z(r_m, \omega_k)|}{\max_{\omega_l \in \Omega} \sum_{m=1}^M |Z(r_m, \omega_l)|} \quad (12)$$

where Ω represents the set of all K tonal frequencies processed.

With α_k estimated, an ML estimate of I_{\max} for each striation is obtained as follows. First, let p be an index corresponding to a particular striation projected across the $|Z(r, \omega)|$ surface and $\mathbf{y}(p, \beta_{\text{hyp}})$ be a K -vector of scaled intensity measurements taken along the p th striation projected using a hypothesized value of β , with components defined as follows:

$$y_k(p, \beta_{\text{hyp}}) \triangleq \frac{|Z(r_k, \omega_k; p, \beta_{\text{hyp}})|^2}{\widehat{\sigma}_n^2(\omega_k)} \quad (13)$$

where the notation $Z(r_k, \omega_k)$ has been expanded to $Z(r_k, \omega_k; p, \beta_{\text{hyp}})$ to indicate a particular locus of points obtained from applying (7) to the $|Z(r, \omega)|$ surface using specific values of p and β_{hyp} . Under the assumption that noisy intensity measurements along a striation are statistically independent, which is in accordance with the source model in (2) given a linear channel and independent additive noise, the likelihood of a hypothesized maximum striation value I_{hyp} is the joint density of the scaled measurements $\mathbf{y}(p, \beta_{\text{hyp}})$ along the striation and is written as

follows:

$$\ell(I_{\text{hyp}} | \mathbf{y}(p, \beta_{\text{hyp}})) = \prod_{k=1}^K f_Y(y_k(p, \beta_{\text{hyp}}); \lambda_k(I_{\text{hyp}})) \quad (14)$$

where λ_k is parameterized by the hypothesized striation intensity as follows:

$$\lambda_k(I_{\text{hyp}}) = \frac{\hat{\alpha}_k^2 I_{\text{hyp}}}{\widehat{\sigma}_n^2(\omega_k)} \quad (15)$$

The ML estimate of the maximum received signal intensity along a particular striation is obtained through an iterative search process and is expressed as follows:

$$\hat{I}_{\text{ML}}(p, \beta_{\text{hyp}}) = \arg \max_{I_{\text{hyp}}} \ell(I_{\text{hyp}} | \mathbf{y}(p, \beta_{\text{hyp}})). \quad (16)$$

The ML intensity estimator derived here is central to both the β estimator presented in Section II-C and the range estimator in Section II-D.

C. ML β Estimation

The ML estimate of β is obtained through a parameter search process, assuming source range is known, as outlined in Fig. 2. Let β_{hyp} denote one of the L hypothesized β values under consideration at a given step of the search. For each hypothesized β , a series of P curves are projected through frequency and range across the $Z(r, \omega)$ surface, which is obtained by computing a spectrogram of the measured hydrophone data and subsequently mapping time to source range. The striations are projected in accordance with (7), using β_{hyp} in place of β . For each projected striation, the ML estimate of noise-free intensity is estimated in accordance with (16), and the likelihood of a particular β_{hyp} is the product of likelihoods of the P curves

$$\ell(\beta_{\text{hyp}}) = \prod_{p=1}^P \ell(\hat{I}_{\text{ML}}(p, \beta_{\text{hyp}}) | \mathbf{y}(p, \beta_{\text{hyp}})). \quad (17)$$

The ML estimate of β is obtained by maximizing this likelihood as

$$\hat{\beta}_{\text{ML}} = \arg \max_{\beta_{\text{hyp}}} \ell(\beta_{\text{hyp}}). \quad (18)$$

D. ML Range Estimation

In Section II-C, a method was presented by which β can be estimated from the time–frequency spectrum of the measured hydrophone data when the time-varying source range is known. In this section, however, it is instead assumed that the time-varying source range is unknown, but the source range rate and β are known. Using knowledge of those two parameters, source range can be estimated in a similar manner to the β estimation technique described previously. The range estimation technique is now presented, beginning with the process by which a spectrogram magnitude surface $|Z(t, \omega)|$ is mapped to a $|Z(r, \omega)|$ surface without knowledge of the source range.

With an estimate of the time-varying source range rate $\hat{v}_{\text{rs}}(t)$, a time–range mapping can be constructed by hypothesizing an

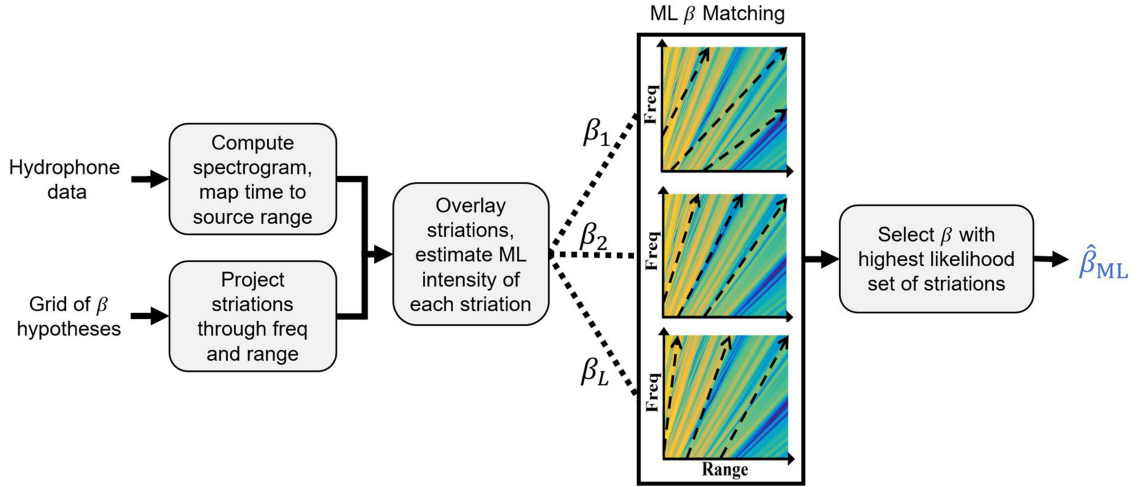


Fig. 2. Block diagram showing an overview of the β estimation process. First, a spectrogram is computed from the hydrophone data, and the resulting time axis is mapped to source range. Striations are computed using (7) for each of L hypothesized β values and are overlaid on the spectrogram. The ML intensity along each striation is computed using (16), and the likelihood of each set of striations, corresponding to a particular hypothesized β , is computed using (17). Finally, the hypothesized β with the highest likelihood is selected. In the example shown in the figure, the second hypothesized β yields a set of projected striations that match closely with those in the spectrogram and would have a relatively high likelihood compared to mismatched hypotheses.

initial source range r_0 at time t_0 . The mapping is computed as follows:

$$r_{\text{hyp}}(t, r_0) = r_0 + \int_{t_0}^t \hat{v}_{\text{rs}}(\tau) d\tau. \quad (19)$$

Using AIS data, which provides time-varying source position $\mathbf{x}_s(t)$ and velocity $\mathbf{v}_s(t)$, and an initial estimate of the receiver position relative to the source, $\hat{\mathbf{x}}_r(t)$, the source range rate is computed as follows:

$$\hat{v}_{\text{rs}}(t) = \frac{\hat{\mathbf{v}}_{\text{rs}}(t) \cdot \hat{\mathbf{x}}_{\text{rs}}(t)}{\|\hat{\mathbf{x}}_{\text{rs}}(t)\|_2} \quad (20)$$

where $\hat{\mathbf{x}}_{\text{rs}}(t) \triangleq \mathbf{x}_s(t) - \hat{\mathbf{x}}_r(t)$, $\hat{\mathbf{v}}_{\text{rs}}(t)$ is the time-varying receiver velocity estimate provided by onboard equipment such as an IMU, $\hat{\mathbf{v}}_{\text{rs}}(t) \triangleq \mathbf{v}_s(t) - \hat{\mathbf{v}}_r(t)$, and $\|\cdot\|_2$ indicates the Euclidean norm. The time-varying receiver position $\hat{\mathbf{x}}_r(t)$ is the sum of two parts: an initial position $\hat{\mathbf{x}}$ and a time-varying displacement $\hat{\mathbf{s}}(t)$ given as follows:

$$\hat{\mathbf{s}}(t) = \int_{t_0}^t \hat{\mathbf{v}}_r(\tau) d\tau. \quad (21)$$

Other methods can also be used to obtain $\hat{v}_{\text{rs}}(t)$ without the requirement of AIS data or estimates of the receiver position and velocity. One such example is the “source differencing” technique proposed by Rakotonarivo and Kuperman [21] in which the source velocity in the same SWellEx-96 data set analyzed in this paper was estimated with an accuracy of ± 0.3 m/s. Alternatively, if the source track exhibits the CPA, then Hough-transform-based techniques can be applied to the $|Z(t, \omega)|$ surface to estimate the ratio of source velocity to range at CPA, as in the work of Tao *et al.* [5].

Once the time–range mapping has been performed, P striations are projected across the corresponding $|Z(r_{\text{hyp}}(t, r_0), \omega)|$ surface in accordance with (7) for each hypothesized initial source range r_0 . The measured intensities at each point along

the p th projected striation are scaled using estimated noise variance $\hat{\sigma}_n^2(\omega)$ and are denoted by the K -vector $\mathbf{y}(p, \beta, r_0)$. The ML estimate of the maximum striation intensity is computed as in (16), and the likelihood of a particular range hypothesis r_0 is the product of likelihoods for each of the P corresponding striations

$$\ell(r_{\text{hyp}}(t, r_0)) = \prod_{p=1}^P \ell(\hat{I}_{\text{ML}}(p, \beta_{\text{hyp}}, r_0) | \mathbf{y}(p, \beta_{\text{hyp}}, r_0)). \quad (22)$$

The ML estimate of source range at time t is as follows:

$$\hat{r}_{\text{ML}}(t) = \arg \max_{r_0} \ell(r_{\text{hyp}}(t, r_0)). \quad (23)$$

E. Simulation

The KRAKEN normal mode ocean acoustic simulation program [22] was used to model a shallow-water Pekeris environment with range-independent bathymetry, 200-m column depth, and an isovelocity sound-speed profile (SSP). This environment was chosen because it is known to be well characterized by $\beta = 1$ [17], and the mean $\hat{\beta}_{\text{ML}}$ obtained by the estimator is expected to be nearly unity.

The channel response magnitude was computed for a midcolumn hydrophone at frequencies between 100 and 200 Hz and at ranges from 2.5 to 7 km, similar to the experimental setup described in Section III-A. β was estimated using the method presented in Section II-C, and a representative plot of the log-likelihood of various hypothesized β values is shown in Fig. 3(a) for a particular realization at an SNR of 20 dB, defined here as the mean value of λ_k for each tonal component. The distribution of β is seen to be sharply peaked near $\beta = 1$, as expected, and the mean value of β obtained from repeated trials was 1.003. This indicates excellent agreement with the canonical $\beta \approx 1$ shallow-water value and lends credibility to the estimator.

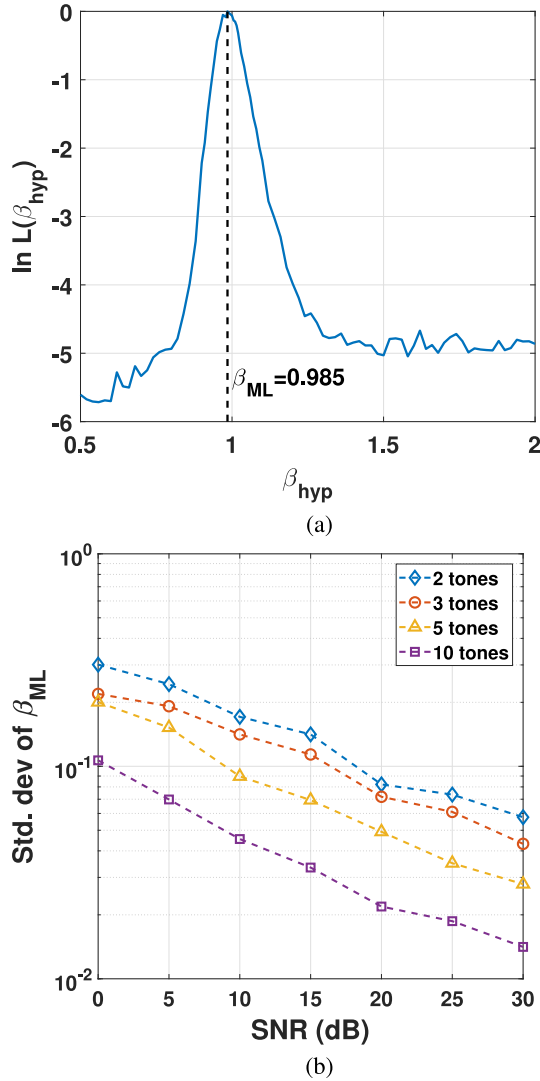


Fig. 3. β estimation results for a simulated shallow-water Pekeris environment. (a) Log-likelihood of hypothesized β values for a single realization at a signal-to-noise ratio (SNR) of 20 dB using five tones. (b) Standard deviation of the ML estimate of β , computed from 175 Monte Carlo trials at each combination of SNR and number of tones processed.

To investigate the impact of SNR and number of tones processed on estimator performance, 175 Monte Carlo trials were conducted at each of 7 SNRs evenly spaced between 0 and 30 dB using 2, 3, 5, and 10 tones. 0–5 dB is the approximate SNR corresponding to typical tones above 200 Hz in the received spectrum of a fast-moving ship, whereas 10–30 dB SNR is more representative of the lower frequency tones between 20 and 100 Hz of a slow-moving ship [12]. Similarly, a typical ship generates about ten tones in the 20–100-Hz spectrum, but only three to seven tones per 100 Hz at higher frequencies [19]. A minimum of two tones are required for waveguide-invariant-based β and range estimation, and performance improves with SNR and number of tones processed, as shown in Fig. 3(b). For the Pekeris environment, the standard deviation of $\hat{\beta}$ is seen to vary from about 0.02 for an optimistic scenario using ten tones at an SNR of 25 dB to a standard deviation of 0.2 when only three tones are processed at an SNR of 5 dB.

To put the β estimation performance into perspective, a standard deviation of 0.02 in $\hat{\beta}$ corresponds to an average receiver position error of around 200 m (using the range estimator presented in Section II-D and the position estimator in Section II-F with source parameters set to mirror those from the experiment described in Section III-A), whereas a standard deviation of 0.2 produced a position error of about 1.3 km. A conservative assumption of processing five tones at an SNR of 10 dB results in a standard deviation of 0.09, which corresponds to a position error of roughly 700 m. However, in real environments, the standard deviation of $\hat{\beta}$ is likely to be slightly higher for a given SNR and number of tones processed due to the more diffuse underlying distribution of β values, as discussed in greater detail in Section III-C.

F. Nonlinear Least-Squares (NLLS) Based Receiver Localization

The ML estimates of the time-varying range to a transiting cargo ship, described in Section II-D, can be combined with knowledge of the source track, obtained from the AIS data, to localize the receiver using an NLLS technique. In practice, this could be used for AUV localization, where the receiver is collocated with the AUV. Let $\hat{\mathbf{x}}_r = [\hat{x}_r, \hat{y}_r]^T$ represent the estimated AUV position vector in 2-D, defined as follows:

$$\hat{\mathbf{x}}_r = \arg \min_{\mathbf{x}_{\text{hyp}}} \|\mathbf{f}(\mathbf{x}_{\text{hyp}})\|_2 \quad (24)$$

where $\mathbf{f}(\mathbf{x}) = [f_1(\mathbf{x}), \dots, f_Q(\mathbf{x})]^T$ is a Q -vector of residuals defined as follows:

$$f_q(\mathbf{x}) = \|\mathbf{x}_s(t_q) - (\mathbf{x} + \hat{\mathbf{s}}(t_q))\|_2 - \hat{r}_{\text{ML}}(t_q). \quad (25)$$

Geometrically, the output of the f_q function is the distance from a hypothesized AUV position, $\mathbf{x}_{\text{hyp}} + \hat{\mathbf{s}}(t)$, to a circle of radius $\hat{r}_{\text{ML}}(t)$ centered at the source position $\mathbf{x}_s(t)$ at time t_q . The least-squares solution $\hat{\mathbf{x}}_r$ can be obtained using a variety of techniques and will not generally be computationally expensive for small values of Q , such as $Q = 19$ used in this work.

If the source track is linear over the observation interval, (24) will yield two solutions that are symmetric with respect to the track axis. However, it is assumed that one of the two solutions will be significantly closer to an initial estimate of the AUV position, provided by an onboard IMU, and the closer of the two solutions would be chosen in such cases. Receiver localization results from the SWellEx-96 experiment, presented in the context of AUV navigation, are provided in Section IV.

III. EXPERIMENT AND RESULTS

The time-varying range from a stationary hydrophone to a transiting tonal source was estimated by processing acoustic data from Event S5 of the SWellEx-96 experiment. Estimating β is a critical part of this process, and while there are several means by which this parameter could be obtained by an AUV, only two are investigated in this section. One method, similar in concept to that employed by Bonnel *et al.* [23], is to use prior knowledge of the environment to estimate β via simulation using a normal mode program, and this is covered in Section III-C.

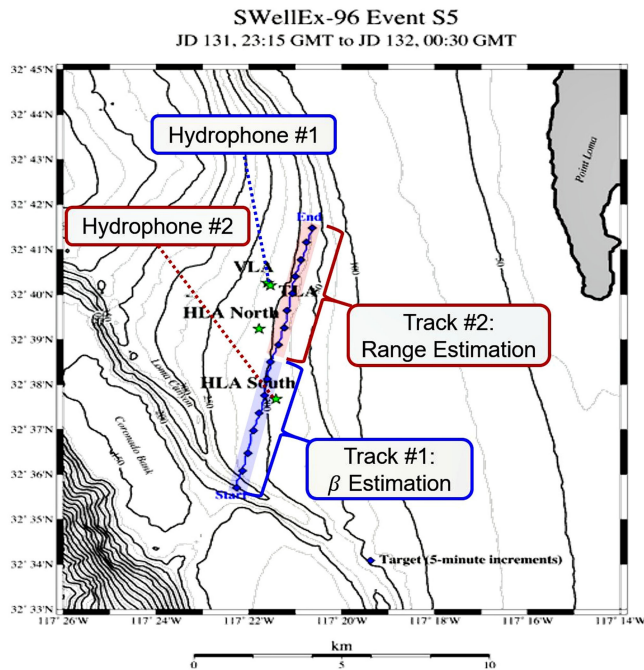


Fig. 4. Overview of the source track, hydrophone positions, and bathymetry for Event S5 of the SWellEx-96 experiment. Bathymetry isolines, drawn every 25 m, are indicated by the alternating thick black and thin gray curves. The source track is indicated by the blue diamonds and is marked at 5-min intervals. The hydrophones utilized for processing data from Tracks #1 and #2 were located within the arrays labeled TLA and HLA South, respectively, and each of the four arrays that were present during the experiment are marked with green stars. The source track was partitioned into two subtracks: the first (shaded blue) is used to estimate β and the second (shaded red) is used to estimate the source range and receiver position. Image credit: <http://swellEx96.ucsd.edu/s5.htm>.

The other method investigated is to estimate β from $|Z(r, \omega)|$, as in Section II-C, which requires knowledge of source range. With access to AIS data and a good estimate of its own position, such as could be obtained when surfacing periodically for GPS, the range to a nearby SOO could be computed, allowing β to be accurately estimated. However, due to the rate at which SOOs typically transit shipping lanes, a different SOO track would likely be used for receiver localization than was used for β estimation. For this reason, the source track in Fig. 4 is partitioned into two subtracks, with the first being used to estimate β and the second being used to estimate source range and subsequently localize the receiver.

Sections III-A and III-B cover the experimental geometry, measured environmental parameters, and source characteristics. Following that, simulation results are presented for β and range estimation for the SWellEx-96 environment in Sections III-C and III-D. Finally, experimental results are presented in Section III-E and are shown to be in close agreement with those obtained through simulation for the second track.

A. Experiment Environment and Geometry

Event S5 of the SWellEx-96 experiment took place in the afternoon of May 10, 1996 in shallow water about 12 km off the tip of Point Loma, California [24]. A cross section of the environment is depicted in Fig. 5 along with parameters of interest such as SSP, which is downward refracting, as well

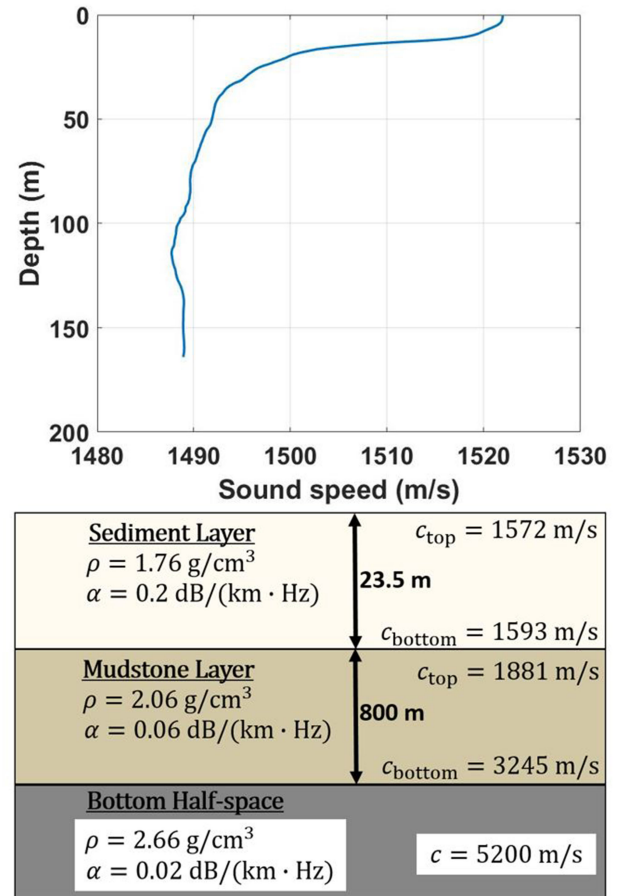


Fig. 5. Graphical depiction of a cross section of the simulated SWellEx-96 environment. SSP is shown at top and was obtained using Station #5 CTD data. Bottom properties include layer depth, density, attenuation, and sound speed. Parameters shown were obtained from the SWellEx-96 website [24].

as various bottom properties. The SSP shown was measured at Station #5, which was selected for its spatial and temporal proximities to Event S5.

During Event S5, which was approximately 75 min in duration, the GPS-equipped research vessel R/V Sproul traveled northeast along the roughly 10-km track shown in Fig. 4 at a rate of 2.5 m/s. The vessel towed a shallow source at a depth of 9 m and a deep source at a depth of 54 m, but the deep source was not utilized for β or range estimation. Although the time-varying position of the tow ship was known from the GPS data, the position of the shallow source was not recorded. Based on matched field processing and other spectral analysis of the hydrophone data, which are not described in this work, the authors estimated that the shallow source lagged behind the tow ship by approximately 13 s, and this offset was applied to the GPS data to estimate the time-varying source position.

The bathymetry over the first half of the total track, herein referred to as Track #1, varies between roughly 275 and 200 m, whereas Track #2 aligns fairly well with the 180-m isobath. Although four fixed arrays of 16 hydrophones recorded the event, only the data from the last hydrophone in the tilted line array (TLA) and the first hydrophone in the horizontal line array south (HLAS) were processed, and these hydrophones are herein referred to as Hydrophone #1 and Hydrophone #2, respectively.

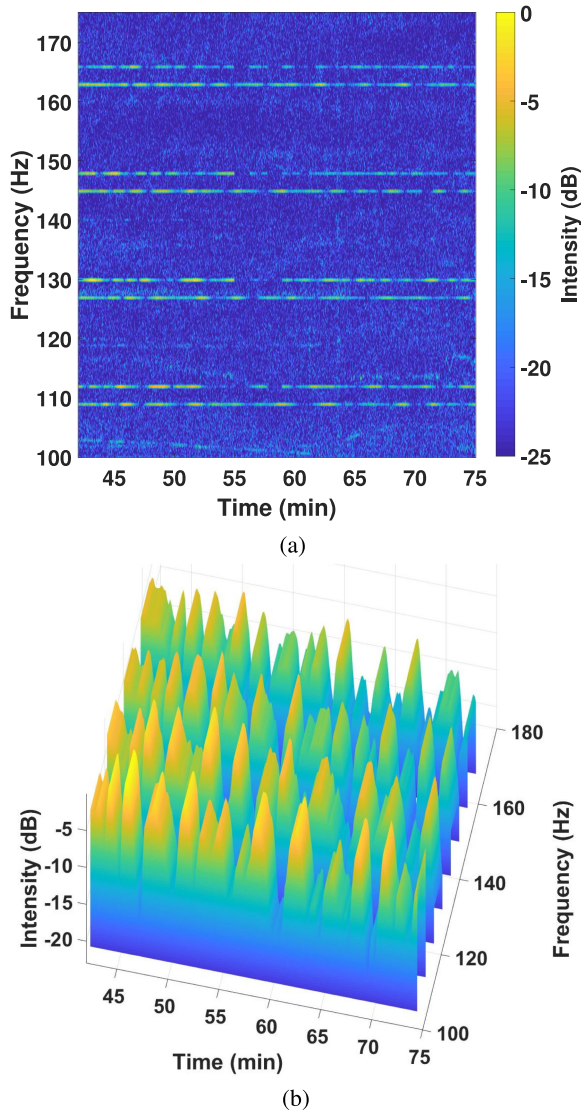


Fig. 6. (a) Spectrogram of the data recorded by Hydrophone #2 during Track #2 of Event S5 of the SWellEx-96 experiment, normalized to 0 dB. The plot shows four pairs of tones between 110 and 170 Hz. The lower frequency tone in each pair corresponds to the shallow source, and the upper tone corresponds to the deep source. (b) Cuts from the spectrogram at left are plotted in 3-D to emphasize the fading pattern in the shallow source tones at [109, 127, 145, 163] Hz used for range estimation.

Hydrophone #1 was located at a depth of 67 m, and Hydrophone #2 at a depth of 198 m. β is known to vary in response to changes in bathymetry between source and receiver [25], as well as receiver depth [26], and splitting the track and data in this manner thus presents a significant challenge to employing the waveguide invariant for range estimation and receiver localization.

B. Source Signal

The shallow source emitted a set of nine tones ranging from 109 to 385 Hz in frequency. The time–frequency spectrum of the signal received at Hydrophone #2 during the second half of the source tow is shown in Fig. 6(a) for 100–175 Hz. Four pairs of tones are distinctly visible in the spectrogram with a 3-Hz spacing between tones in each pair. The higher frequency

tone in each pair was transmitted by the deep source and the lower frequency tone by the shallow source. Unlike the shallow source, which transmitted tones continuously throughout the experiment, the deep source ceased its tonal emissions for about a minute at both 55 and 58 min into the experiment, and the corresponding portions of the spectrogram in Fig. 6(a) thus resemble nulls in the fading pattern.

Only the four lowest frequency tones present in the shallow source signal were used for waveguide-invariant-based range estimation, and the fading pattern observed in these tones is shown in Fig. 6(b). The lowest frequency tones were chosen primarily because SOOs have been observed to exhibit strong tonal emissions at lower frequencies [19], especially when traveling at lower speeds [12].

C. Simulation: β Estimation

In addition to the isovelocity channel used in Section II-E, a more realistic environment was also simulated in which the SSP and bottom properties used in KRAKEN matched those that were measured during Event S5 of the SWellEx-96 experiment [24]. In this environment, the receiver was located below the thermocline at the bottom of the water column, at a depth of 163 m. Note that the approximate depth of the hydrophones belonging to HLAS was 198 m, but 163 m was used in simulation as that was the depth of the water column at which the Station #5 conductivity, temperature, depth (CTD) cast took place. This environment was used to separately estimate both β and source range, although in practice, the same track would not generally be used to estimate both parameters, as knowledge of one is required to obtain the other.

To estimate β , a 4.5-km source tow was simulated at five frequencies evenly spaced between 110 and 170 Hz, which is approximately the span of source frequencies utilized from the SWellEx-96 data. With a simulated shallow source at 9-m depth, β is estimated to be 1.20, as shown in Fig. 7(a). In comparison to Fig. 3(a), the peak in Fig. 7(a) is broader, and this corresponds to a more diffuse distribution of β values, as noted by Rouseff [26] and Turgut *et al.* [27] for environments in which the receiver is located below the thermocline. However, as noted in [27], the broadening of the peak is moderated when the source is located above the thermocline, as it would be in the case of SOOs, such as cargo ships, and the mode of the distribution does not tend to shift far from unity. For AUVs operating near shipping lanes, the relative stability of the distribution could potentially allow for range estimation and receiver localization to be performed without requiring the vehicle to maintain a constant depth.

The performance of the estimator was analyzed using various numbers of tones and SNRs, as in Section II-E, and the sample standard deviation for each set of 175 Monte Carlo trials is plotted in Fig. 7(b). Across all combinations of parameters tested, an average increase of 23% was observed in the standard deviation of $\hat{\beta}$ compared to the results obtained for the Pekeris environment [see Fig. 3(b)]. Thus, despite the moderate broadening of the β distribution compared to the Pekeris environment, a fairly low variance in β estimates should be seen when processing portions of the SWellEx-96 data for which the environment is relatively range independent, as it was in simulation.

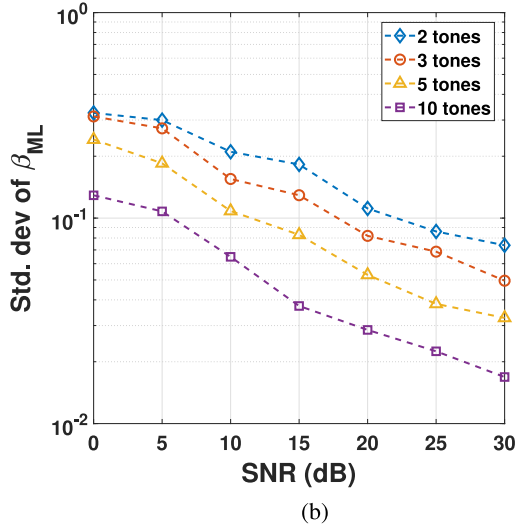
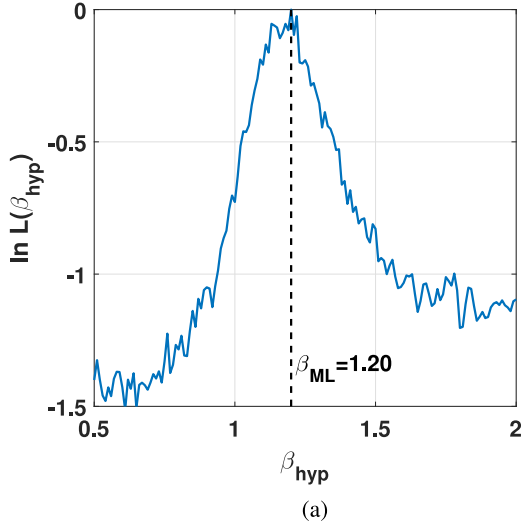


Fig. 7. β estimation results for the simulated SWellEx-96 shallow-water environment, with 163-m column depth and experimentally measured SSP and bottom properties. (a) Log-likelihood of hypothesized β values for a single realization at an SNR of 20 dB. (b) Standard deviation of $\hat{\beta}_{ML}$, computed from 175 Monte Carlo trials at each combination of SNR and number of tones processed.

D. Simulation: Range Estimation

Before analyzing the experimental data, source range was estimated using the same, simulated SWellEx-96 environment that was used previously for β estimation. The previously obtained mean ML estimate of the waveguide invariant parameter over the entire 4.5-km source track, $\hat{\beta} = 1.20$, was used for range estimation. However, to facilitate a more direct comparison of the simulation results to those obtained from processing the real data, the source track was shortened to 2.1 km, which corresponds to a 15-min time interval with an average source range rate of 2.3 m/s, approximately matching the typical data segment processed from Track #2 of the experimental data.

For the selected range estimation trial shown in Fig. 8(a), the true source range was 2.5 km, and the ML range estimate at an SNR of 20 dB is 2.57 km, with an error of about 3%. The standard deviation of the range estimator as a function of SNR is shown in Fig. 8(b) and is seen to be approximately 120 m

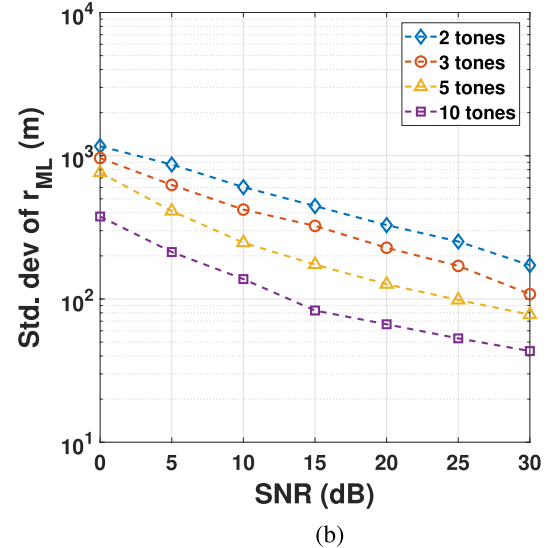
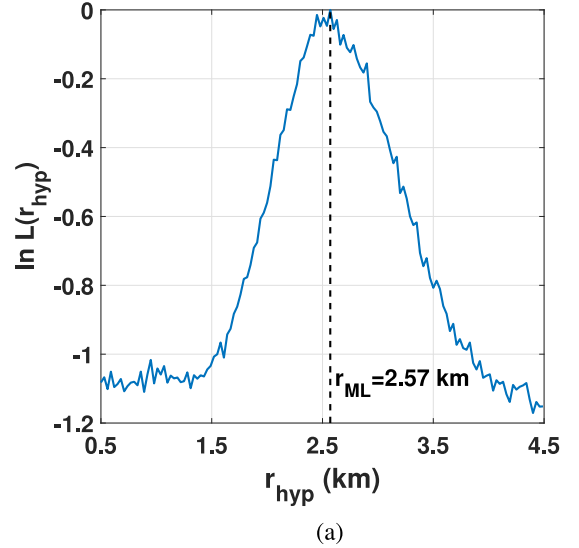


Fig. 8. (a) Log-likelihood of the hypothesized initial source range r_{hyp} for a simulated 2.1-km track in the SWellEx-96 environment. True initial source range was 2.5 km, and the estimated range is seen to be 2.57 km. (b) Standard deviation of ML estimate of the initial source range, computed from 175 Monte Carlo trials at each combination of SNR and number of tones processed.

at 20 dB SNR using five tones. At an SNR of 13.7 dB, which is the average from the SWellEx-96 experiment, the standard deviation increases to just over 200 m.

E. SWellEx-96 Range Estimation Results

In this section, real data from the SWellEx-96 experiment is used to produce ML estimates of time-varying source range. The noise variance parameter $\sigma_n^2(\omega)$ was estimated using the following frequency components in the spectrograms: [107 125 143 161] Hz. The average SNR for the processed data was 13.7 dB, with a peak of 14.8 dB for the 39–54-min window and a minimum of 10.8 dB for the last window covering the experiment time frame of 60–75 min. The $\hat{\alpha}_k$ values computed using (12) ranged from -0.1 to 0 dB, which is not surprising given that all tones in the source signal that were selected for

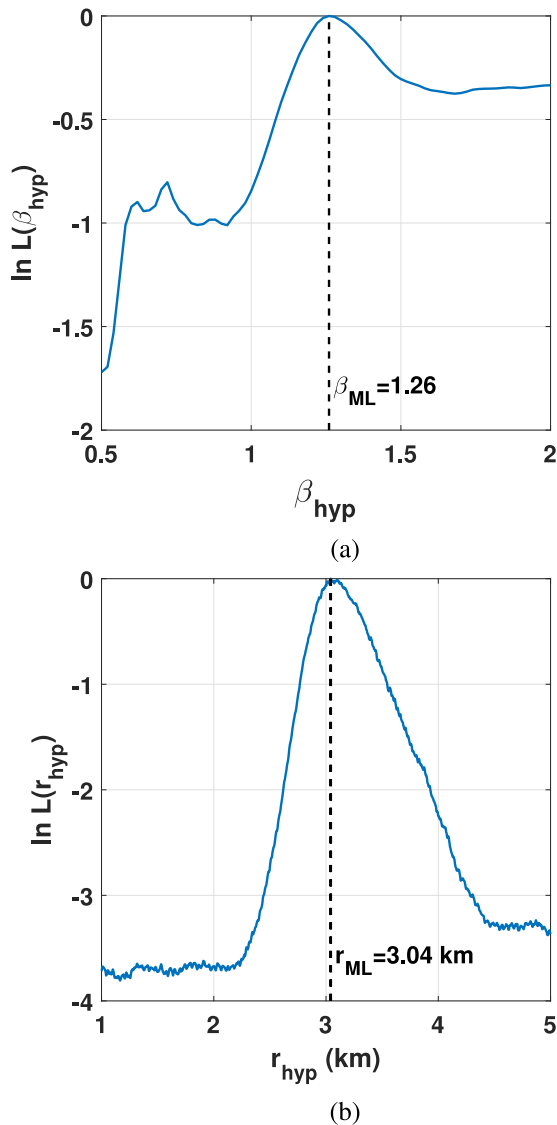


Fig. 9. Log-likelihood of hypothesized parameters obtained from processing selected segments of the SWellEx-96 data. (a) Hypothesized β values for a 20-min segment of data from Hydrophone #1 over Track #1 for which β is estimated to be 1.26. (b) Hypothesized source ranges for a 15-min segment of data recorded by Hydrophone #2 from Track #2. True initial source range was 2.92 km and the ML range is seen to be 3.04 km, using the estimate $\hat{\beta}_1 = 1.26$ obtained previously from Track #1.

processing were transmitted at the same level of 158 dB re 1 uPa [24].

As mentioned previously, there are multiple ways to obtain the requisite estimate of β , and we begin by using data acquired from Hydrophone #1 to estimate β over Track #1. The mean value of the waveguide invariant estimated over the 40-min track, referred to as $\hat{\beta}_1$, was 1.26. The log-likelihood of various hypothesized β values for a 20-min portion of data covering the middle of Track #1 is plotted in Fig. 9(a). The distribution of β values is much less concentrated near the mode than it was in simulation, and this is likely due to the rapidly varying bathymetry over the track.

Source range was estimated using data from Hydrophone #2 covering Track #2 assuming $\beta = 1.26$, and the log-likelihood

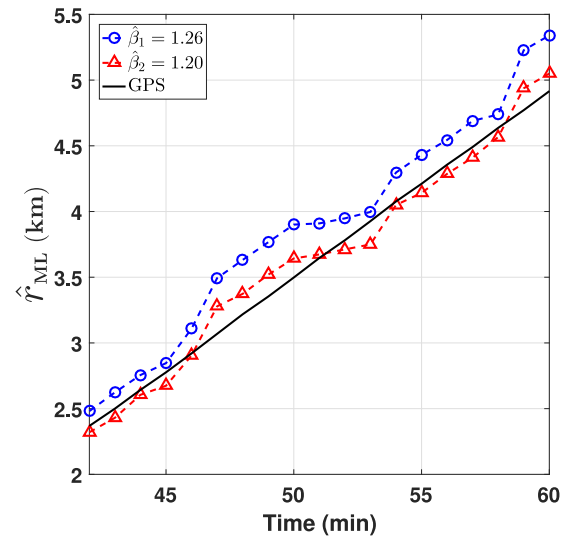


Fig. 10. ML source range over Track #2 plotted against the true, GPS-derived range to the shallow source as a function of experiment time. The blue circles correspond to range estimates obtained using the value of β estimated from processing acoustic data from Track #1 while the red triangles correspond to using the value of β estimated from Track #2. Acoustic data were processed independently in 15-min blocks, and estimated range corresponds to the source-receiver range at the beginning of a block.

of various hypothesized source ranges for a 15-min window of data beginning at 46 min is plotted in Fig. 9(b). Additionally, data from Hydrophone #2 were also used to estimate β over Track #2, using knowledge of source range, and this yielded a mean estimate $\hat{\beta}_2 = 1.20$, which is identical to the value obtained through simulation using KRAKEN in Section III-C. The ML range estimates obtained from processing Track #2 in overlapping 15-min blocks are overlaid in Fig. 10 for both estimates of β . The mean error in range estimates using $\hat{\beta}_1$ was 240 m, compared to only 9 m when using $\hat{\beta}_2$. The impact of an error in $\hat{\beta}$ is thus seen to be a shift in the range estimates, which follows from (7). The standard deviation of range estimation error was 115 m using $\hat{\beta}_2$ and 140 m using $\hat{\beta}_1$. These results are lower than the value of 200 m predicted from simulations, and the difference could be due to the small sample size of the experimental data. Nevertheless, the results indicate that this environment is fairly well characterized by a single value of β , despite the receiver being located below the thermocline, and the range estimates obtained from using $\hat{\beta}_1$ could prove useful for receiver localization.

IV. AUV LOCALIZATION

In this section, the source range estimates obtained from processing acoustic data from Track #2 in Section III-E are applied to AUV navigation by demonstrating the potential to localize a submerged AUV using a combination of hydrophone, AIS, and IMU data. To this end, Hydrophone #2 is considered to be located inside a submerged AUV, and the data it recorded during the SWellEx-96 experiment will be used to estimate the position of the vehicle. Furthermore, the IMU onboard the AUV is assumed to have a velocity estimation error due to factors such

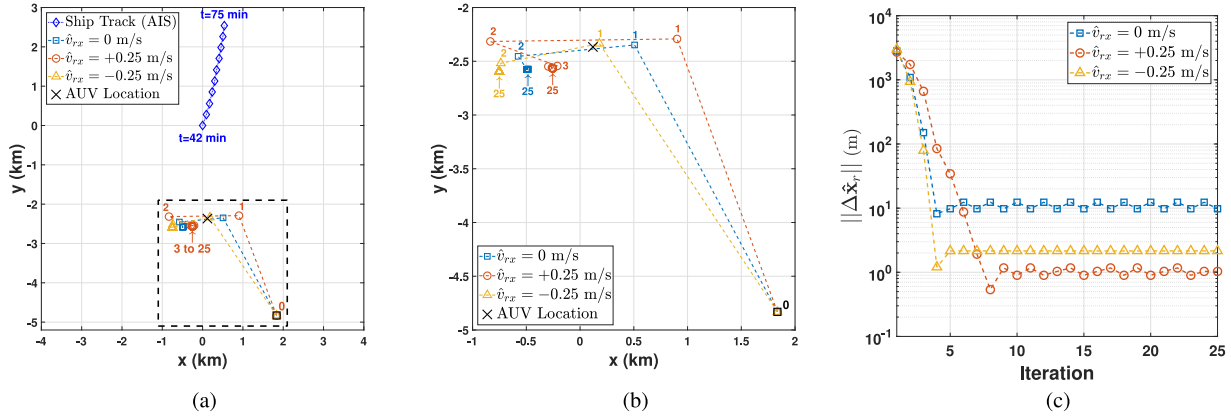


Fig. 11. Results for the first 25 iterations of the NLLS-based receiver localization algorithm using various estimates of the x -component of the receiver velocity \hat{v}_{rx} . (a) Localization results shown relative to ship track, indicated by the blue diamonds, and initial location estimate provided by the IMU, indicated by the solid black square labeled “0” at (1.8, -4.8) km. The portion of the figure bounded by the dashed box is enlarged in (b), with points indicating the location estimates obtained at the end of the iterations specified by accompanying color-coded numerical labels. (c) Plot of the distance, in meters, between subsequent NLLS estimates of AUV position.

as underwater currents and accelerometer drift, despite actually being moored to ocean floor during the experiment.

For real-time AUV localization, the method would be contingent upon a processor onboard the AUV having access to time-varying source position information, such as that contained in AIS data. This can be accomplished by having a surface buoy receive radio frequency AIS broadcasts from nearby transiting cargo ships and then relay the data acoustically to submerged assets using the JANUS protocol, as demonstrated during the REP15-Atlantic and REP16-Atlantic sea trials with successful AIS data transmissions at distances up to 5.5 km [28]. Another potential application is post-mission AUV localization, or reconstruction analysis, in which the objective is to estimate the track that was transited by an underwater vehicle between deployment and recovery. For that application, the AIS data can be readily obtained from various online databases after recovery, without the need for real-time AIS-relaying mechanisms.

A. Localization Algorithm and Scenario

The process by which the AUV position is estimated is as follows: first, the source range rate is computed using (20) based on data provided by the IMU. Next, the waveguide-invariant-based range estimation processor uses an estimate of β for the environment, combined with the source range rate estimates, to produce a sequence of time-varying ML range estimates using (23). Finally, the AUV position hypothesis is updated using the estimate obtained from (24), and the process is repeated. After several iterations, the mean position estimate begins to converge, and the AUV position can be estimated once a desired change threshold has been met.

A scenario is now presented in which an AUV has been submerged for over an hour, and the onboard IMU provides an erroneous position estimate 3 km southeast of its true location, as shown in Fig. 11(b), in addition to a velocity estimate with an error of 0.25 m/s. A position error of this magnitude is consistent with what could be expected for a low-cost, standalone IMU [1], and the velocity error would, in reality, be scaled higher by a

factor roughly equal to the ratio of average cargo ship speed to the speed of the source towed in the SWellEx-96 experiment, which is about 5. Thus, the 0.25-m/s velocity estimation error assumed in this scenario would produce a similar effect to an error of 1.25 m/s when using a cargo ship SOO.

B. Results

The erroneous AUV position and velocity estimates obtained from the IMU lead to an error in source range rate $\hat{v}_{rs}(t)$, as shown by the plot corresponding to the first iteration in Fig. 12(a). The waveguide-invariant-based range estimator subsequently produces the series of range estimates corresponding to the first iteration in Fig. 12(b). The NLLS estimate of receiver position, indicated by the red “1” in Fig. 11(b) is about 800 m east of the true AUV position. This updated position estimate is 2.8 km away from the initial position estimate provided by the IMU, as indicated by the red circle corresponding to the first iteration in Fig. 11(c). At this point, the first iteration is completed, and the AUV position hypothesis is updated. The first iteration yields range and range rate hypotheses that are much closer to ground truth than those computed directly from the IMU data, as indicated by the plots corresponding to Iteration #2 in Fig. 12(a) and (b). Successive iterations produce progressively smaller changes in estimated position, as shown in Fig. 11(c), with a distance of only 1 m separating subsequent runs beyond Iteration #8 for this scenario. The final position estimate is 0.43-km southwest of the true AUV position, which is a marked improvement over the error of 3 km in the estimate provided by the IMU. Results obtained using other source velocity errors are shown in Fig. 11 and include an error of 0.64 km when correctly assuming a stationary AUV and an error of 0.9 km when assuming a velocity of 0.25 m/s due west ($\hat{v}_{rx} = -0.25$ m/s).

C. Discussion of Results

This result shows promise for AUV navigation applications, in which IMU position error grows quadratically with

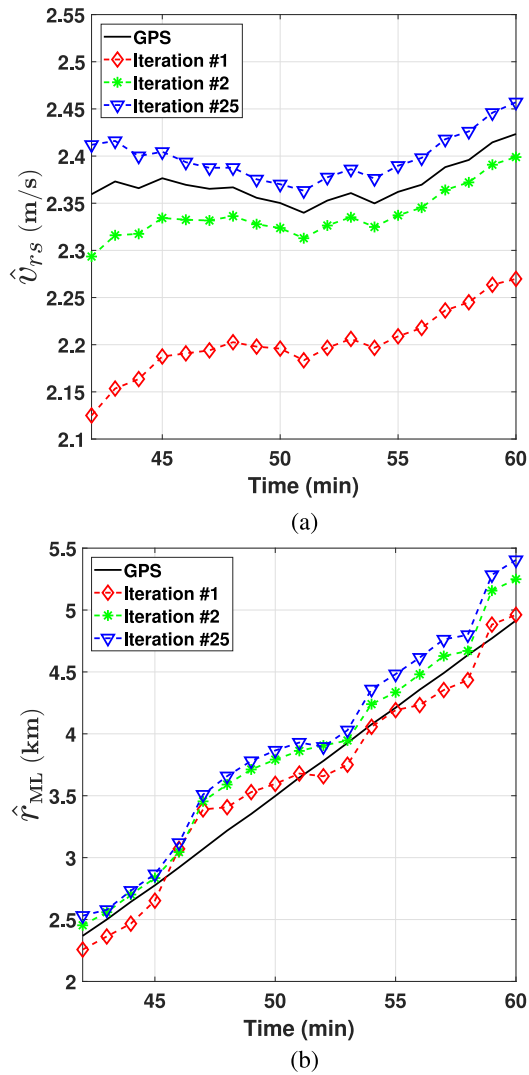


Fig. 12. (a) Estimated source range rate and (b) source range as a function of experiment time for various NLLS iterations using $\hat{\beta}_1 = 1.26$ and assuming a stationary receiver. The first iteration begins with an IMU estimate 3-km southeast of the true AUV position.

time submerged due to accelerometer drift. In contrast to this, the waveguide-invariant-based localization accuracy can be expected to improve with additional measurements of the channel fading pattern as the source transits through an area, assuming the AUV can receive periodic AIS updates. In a high-traffic environment, in which one or more cargo ships transit per hour, an AUV could potentially remain submerged indefinitely while maintaining a position uncertainty of less than 1 km using this localization technique.

The experimental results obtained in this work used data from hydrophones that were located below the thermocline, due to being moored to the ocean floor, and the more diffuse distribution of β values caused a higher variance in range estimates than would otherwise be obtained for a receiver located closer to the surface. Thus, AUVs that have the mission flexibility to operate above the thermocline could potentially benefit from much lower position estimation error. However, as noted in Section III-C, the detrimental impact on AUV localization when operating be-

low the thermocline will be somewhat mitigated by the fact that the propellers and hulls of SOOs are near the top of the water column, and the excitation of higher order, surface-interacting modes helps to anchor the distribution of β values near unity. In principle, an SOO located beneath the thermocline could also be utilized for AUV localization, but β would be much more sensitive to receiver depth, as noted in [8].

D. Application Considerations

The primary advantage of this AUV localization technique over others that are commonly employed is that it requires minimal equipment to be added to the AUV. A single hydrophone could presumably be incorporated at relatively low cost and complexity, and many AUVs are already equipped with one or more hydrophones for signal collection purposes. Furthermore, this technique is passive and does not require any signal transmission by the AUV, thus minimizing its acoustic footprint. In contrast to this, other types of navigation equipment, such as DVLs or acoustic transponders, can be very expensive to equip, require acoustic transmissions by the AUV, and also come with operational limitations. For example, DVLs impose a requirement on the AUV to maintain proximity to the ocean floor, and acoustic transponders require the AUV to remain within a predetermined region of the ocean where the equipment has been previously deployed. In contrast, this technique allows the AUV to transit at a variety of depths within the water column and only requires it to be in proximity to shipping lanes, which translates to a very large potential operating area throughout the world.

The primary impediments to employing this technique are having the infrastructure in place by which AIS data can be relayed to the AUV, as mentioned previously, and in initially characterizing an environment with an estimate of β . The former is not an issue if real-time AUV localization is not a requirement, as in the case of post-mission processing mentioned previously. The latter could potentially be mitigated through prior knowledge of the environment, such as bathymetry and sound speed, or by employing β maps, as proposed in [13]. Further validation using measured acoustic data from cargo ships in shallow-water shipping lanes might help to identify additional advantages and disadvantages relative to conventional localization techniques.

V. CONCLUSION

This paper presented ML estimators for β and source range, along with potential applications to real-time AUV navigation and post-mission AUV localization. The β estimator extended prior work by Harms *et al.* [14] and was validated in multiple ways, beginning with a simulation of a Pekeris environment using KRAKEN and moving on to a simulation of the SWellEx-96 environment, for which the resulting estimate of β matched closely with those obtained from processing the experimental data over two separate tracks. A performance analysis was conducted to examine the impact of SNR and number of tones processed, and the results look promising using parameters that are typical for acoustic emissions of cargo ships. The source range estimator was an extension of the ML β estimator and required an estimate of range rate. The range estimates obtained

from the real data had a standard deviation of under 150 m when processing a source track from 2.5 to 7 km in range. The estimator was further validated by employing an estimate of β obtained from one source track to estimate both source range and receiver position using data recorded from a different track on a hydrophone located 5 km away.

Most importantly, it was shown that AUV localization can potentially be performed using waveguide-invariant-based range estimates combined with knowledge of the source track obtained from AIS data, in either real-time or post-mission settings. Furthermore, the localization technique presented can be performed without knowledge of the source range rate, as this parameter can instead be estimated iteratively from an initial position estimate provided by an instrument, such as a low-grade, onboard IMU. The experimental data suggest that a hydrophone-equipped AUV could use the proposed localization technique to reduce its position estimation error from 3 km to less than 1 km through an iterative nonlinear least-squares-based technique using just four tones from the acoustic emissions of a transiting SOO.

The results presented bode well for applications to AUV navigation in high-traffic, shallow-water environments, such as coastal shipping lanes. With an extension to incorporate broadband striations for increased performance, and with the necessary AIS-relaying infrastructure in place, the technique could potentially enable AUVs to remain submerged indefinitely while maintaining an acceptable position uncertainty in real time. In addition to the broadband extension, future work in this area could include a derivation of the Cramér–Rao bounds for these estimators, field validation using AUVs operating near coastal shipping lanes, and extensions to simultaneously exploit multiple SOOs.

ACKNOWLEDGMENT

The authors would like to thank K. Gemba and D. Ensberg for providing matched field processing data and for helpful discussions to confirm their estimates of the positions of the deep and shallow sources relative to the tow ship in the SWellEx-96 experiment.

REFERENCES

- [1] L. Paull, S. Saeedi, M. Seto, and H. Li, “AUV navigation and localization: A review,” *IEEE J. Ocean. Eng.*, vol. 39, no. 1, pp. 131–149, Jan. 2014.
- [2] S. Chuprov, “Interference structure of a sound field in a layered ocean,” *Ocean Acoustics: Current State*. Moscow, Russia: Nauka, 1982, pp. 71–91.
- [3] H. M. Perez, R. Chang, R. Billings, and T. L. Kosub, “Automatic identification systems (AIS) data use in marine vessel emission estimation,” in *Proc. 18th Annu. Int. Emission Inventory Conf.*, 2009, pp. 1–25. [Online]. Available: <http://www.epa.gov/ttnchie1/conference/ei18/session6/perez.pdf>
- [4] A. M. Thode, “Source ranging with minimal environmental information using a virtual receiver and waveguide invariant theory,” *J. Acoust. Soc. Amer.*, vol. 108, no. 4, pp. 1582–1594, 2000. [Online]. Available: <https://doi.org/10.1121/1.1289409>
- [5] H. Tao, G. Hickman, J. L. Krolik, and M. Kemp, “Single hydrophone passive localization of transiting acoustic sources,” in *Proc. OCEANS Conf. Eur.*, Jun. 2007, pp. 1–3.
- [6] K. L. Cockrell and H. Schmidt, “Robust passive range estimation using the waveguide invariant,” *J. Acoust. Soc. Amer.*, vol. 127, no. 5, pp. 2780–2789, 2010. [Online]. Available: <https://doi.org/10.1121/1.3337223>
- [7] A. Turgut, M. Orr, and D. Rouseff, “Broadband source localization using horizontal-beam acoustic intensity striations,” *J. Acoust. Soc. Amer.*, vol. 127, no. 1, pp. 73–83, 2010. [Online]. Available: <https://doi.org/10.1121/1.3257211>
- [8] D. Rouseff and R. C. Spindel, “Modeling the waveguide invariant as a distribution,” *AIP Conf. Proc.*, vol. 621, no. 1, pp. 137–150, 2002. [Online]. Available: <https://aip.scitation.org/doi/abs/10.1063/1.1486279>
- [9] T. C. Yang, “Beam intensity striations and applications,” *J. Acoust. Soc. Amer.*, vol. 113, no. 3, pp. 1342–1352, 2003. [Online]. Available: <https://doi.org/10.1121/1.1534604>
- [10] K. D. Heaney, “Rapid geoacoustic characterization using a surface ship of opportunity,” *IEEE J. Ocean. Eng.*, vol. 29, no. 1, pp. 88–99, Jan. 2004.
- [11] L. Brooks, M. Kidner, A. Zander, C. Hansen, and Z. Zhang, “Techniques for extraction of the waveguide invariant from interference patterns in spectrograms,” in *Proc. Acoustics*, Nov. 2006, pp. 445–452.
- [12] P. T. Arveson and D. J. Vendittis, “Radiated noise characteristics of a modern cargo ship,” *J. Acoust. Soc. Amer.*, vol. 107, no. 1, pp. 118–129, 2000. [Online]. Available: <https://doi.org/10.1121/1.428344>
- [13] C. M. A. Verlinden, J. Sarkar, B. D. Cornuelle, and W. A. Kuperman, “Determination of acoustic waveguide invariant using ships as sources of opportunity in a shallow water marine environment,” *J. Acoust. Soc. Amer.*, vol. 141, no. 2, pp. EL102–EL107, 2017. [Online]. Available: <https://doi.org/10.1121/1.4976112>
- [14] A. Harms, J. L. Odom, and J. L. Krolik, “Ocean acoustic waveguide invariant parameter estimation using tonal noise sources,” in *Proc. IEEE Int. Conf. Acoust., Speech Signal Process.*, Apr. 2015, pp. 4001–4004.
- [15] A. Young, J. Soli, and G. Hickman, “Self-localization technique for unmanned underwater vehicles using sources of opportunity and a single hydrophone,” in *Proc. OCEANS Conf.*, Anchorage, AK, USA, Sep. 2017, pp. 1–6.
- [16] S. Kay, *Fundamentals of Statistical Signal Processing*, vol. 2. Upper Saddle River, NJ, USA: Prentice-Hall, 2011.
- [17] F. B. Jensen, W. A. Kuperman, M. B. Porter, and H. Schmidt, in *Computational Ocean Acoustics*. New York, NY, USA: Springer, 2011, pp. 133–136.
- [18] A. Papoulis, *Probability, Random Variables, and Stochastic Processes*, 3rd ed. New York, NY, USA: McGraw-Hill, 1991, p. 140.
- [19] S. C. Wales and R. M. Heitmeyer, “An ensemble source spectra model for merchant ship-radiated noise,” *J. Acoust. Soc. Amer.*, vol. 111, no. 3, pp. 1211–1231, 2002. [Online]. Available: <https://doi.org/10.1121/1.1427355>
- [20] M. Evans, N. Hastings, and B. Peacock, *Statistical Distributions*, 3rd ed. New York, NY, USA: Wiley, 2000, p. 169.
- [21] S. T. Rakotonarivo and W. A. Kuperman, “Model-independent range localization of a moving source in shallow water,” *J. Acoust. Soc. Amer.*, vol. 132, no. 4, pp. 2218–2223, 2012. [Online]. Available: <https://doi.org/10.1121/1.4748795>
- [22] M. B. Porter, “The acoustics toolbox,” 2017. [Online]. Available: <http://oalib.hlsresearch.com/Modes/AcousticsToolbox/index.html>, Accessed on: Sep. 9, 2017.
- [23] J. Bonnel, B. Nicolas, J. I. Mars, and D. Fattaccioli, “Source localisation in deep water using waveguide invariant distribution,” in *Proc. 10th Eur. Conf. Underwater Acoust.*, Istanbul, Turkey, Jul. 2010. [Online]. Available: <https://hal.archives-ouvertes.fr/hal-00599607>
- [24] J. Murray and D. Ensberg, “Swellex-96: S5 event,” 1996. [Online]. Available: <http://swellex96.ucsd.edu/s5.htm>, Accessed on Feb. 1, 2017.
- [25] G. L. D’Spain and W. A. Kuperman, “Application of waveguide invariants to analysis of spectrograms from shallow water environments that vary in range and azimuth,” *J. Acoust. Soc. Amer.*, vol. 106, no. 5, pp. 2454–2468, 1999. [Online]. Available: <https://doi.org/10.1121/1.428124>
- [26] D. Rouseff, “Effect of shallow water internal waves on ocean acoustic striation patterns,” *Waves Random Media*, vol. 11, pp. 377–393, 2001.
- [27] A. Turgut, L. T. Fialkowski, and J. A. Schindall, “Measured depth-dependence of waveguide invariant in shallow water with a summer profile,” *J. Acoust. Soc. Amer.*, vol. 139, no. 6, pp. EL184–EL189, 2016. [Online]. Available: <https://doi.org/10.1121/1.4953581>
- [28] R. Petroccia, J. Alves, and G. Zappa, “JANUS-based services for operationally relevant underwater applications,” *IEEE J. Ocean. Eng.*, vol. 42, no. 4, pp. 994–1006, Oct. 2017.



Andrew H. Young received the B.S. degree in electrical engineering from the University of Colorado, Colorado Springs, CO, USA, in 2008, and the M.S. degree in electrical engineering from Duke University, Durham, NC, USA, in 2017, where he is currently working toward the Ph.D. degree in electrical and computer engineering.

He was a Research Assistant with the Sensor Array and Multipath Signal Processing Lab, Duke University. Since 2018, he has been with the Acoustics Division, Naval Research Laboratory, Washington, DC, USA. His research interests include signal processing for radar and sonar applications.

DC, USA. His research interests include signal processing for radar and sonar applications.



H. Andrew Harms received the B.S. (*summa cum laude*) degree in electrical engineering from the University of Notre Dame, Notre Dame, IN, USA, in 2008, and the Ph.D. degree in electrical engineering from Princeton University, Princeton, NJ, USA, in 2013.

He is currently an Assistant Professor at the University of Nebraska-Lincoln, Lincoln, NE, USA. From 2013 to 2016, he was a Postdoctoral Researcher at Duke University, Durham, NC, USA. Additionally, he was also with Air Force Research Labs, working on nonlinear estimation problems and new communication waveforms for the Air Force. His research interests include statistical signal processing, efficient sampling and processing of signals, information theory, and signal processing for radar systems.

ing on nonlinear estimation problems and new communication waveforms for the Air Force. His research interests include statistical signal processing, efficient sampling and processing of signals, information theory, and signal processing for radar systems.

Granger W. Hickman received the Ph.D. degree in electrical engineering from Duke University, Durham, NC, USA, in 2001.

He is currently a Senior Research Scientist at both Duke University and STRAD Corporation, Chapel Hill, NC, USA. His research interests include statistical signal processing in the areas of radar and sonar.



Jeffrey S. Rogers (S'04–M'10) received the B.S. degree in electrical engineering from the University of California at Santa Barbara, Santa Barbara, CA, USA, in 2004, and the M.S. and Ph.D. degrees in electrical and computer engineering from Duke University, Durham, NC, USA, in 2007 and 2010, respectively.

In 2010, he joined the Acoustics Division, Naval Research Laboratory, Washington, DC, USA, as an Electrical Engineer and is currently the Head of the Active Acoustics Section. He is currently an Adjunct Assistant Professor with the Electrical and Computer Engineering Department, Duke University. His research interests include acoustic signal and array processing, ambient noise modeling, information theory, acoustic metamaterials, and novel signal processing methods for acoustic metamaterial devices.

Dr. Rogers is a member of the Acoustical Society of America and Tau Beta Pi. He is currently an Associate Editor for the Acoustical Society of America *Proceedings of Meetings on Acoustics*. In 2017, he was the recipient of the Alan Berman Publication Award (ARPAD) recognizing the most outstanding publications within the Naval Research Laboratory.



Jeffrey L. Kroluk (S'82–M'83–SM'12) received the B.A.Sc. degree in engineering science and the M.S. and Ph.D. degrees in electrical engineering from the University of Toronto, Toronto, ON, Canada, in 1980, 1983, and 1987, respectively.

He is currently a Professor in Electrical and Computer Engineering at Duke University, Durham, NC, USA. Between December 2014 and 2017, he was on leave as a Program Manager from the Defense Advanced Research Projects Agency in its Strategic Technology Office. In 2008, he founded STRAD

Corporation whose mission is to transition radar and sonar signal processing research into real systems for government and commercial applications. Prior to joining Duke in 1992, he held academic positions with the Marine Physical Laboratory of the Scripps Institution of Oceanography, University of California San Diego and Concordia University, QC, Montreal, Canada. His interests include physics-based signal and sensor array processing with applications to radio frequency and acoustic surveillance systems. At Duke, he has led funded research programs in passive and active sonar, wide-area over-the-horizon HF radar, microwave remote sensing, and RF backscatter communications.